Electronic Supplementary Material (ESI) for Environmental Science: Nano.

Electronic Supplementary Information

Tubular nanoreactor directing the formation of *in situ* iron oxide nanorods with superior photocatalytic activity

Sankar Das[a] and Subhra Jana[a,b]*

[a] Department of Chemical, Biological & Macro-Molecular Sciences, [b] Technical Research Centre, S. N. Bose National Centre for Basic Sciences, Block - JD, Sector-III, Salt Lake, Kolkata -700 106, India. E-mail: subhra.jana@bose.res.in

Experimental Section

Materials

All chemicals were used as received. Halloysite nanotubes (HNTs), iron (III) chloride ($FeCl_3$) and 1,4-benzoquinone were received from Sigma-Aldrich. Ethylenediaminetetra acetic acid disodium salt, sodium hydroxide (NaOH), potassium ferricyanide, congo red (CR) and methylene blue (MB) were obtained from Sisco Research Laboratory (SRL), India. Potassium hexacyanoferrate (II) trihydrate, sodium azide and hydrogen peroxide were purchased from Merck.

Characterization

The morphology of halloysite nanotubes (HNTs) was characterized by transmission electron microscope (TEM: FEI TECNAI G2 F20-ST) using an accelerating voltage of 200 kV after drop casting a drop of solution on a carbon coated copper grid. High resolution transmission electron microscope (HR-TEM) and Energy dispersive X-ray spectroscopy (EDX) analyses were carried out in the above mentioned TEM. Fourier transform infrared spectroscopic (FTIR) measurements of the samples were recorded in the range of 500 to 4000 cm^{-1} using JASCO FTIR 6300. All the FTIR spectra were measured in KBr pellets in the transmission mode. No of scans was fixed to 50 with a resolution of 2 cm^{-1}. The solid state ^{29}Si, ^{27}Al, and ^{13}C cross-polarization magic-angle spinning (CPMAS) NMR spectroscopy were performed using a JEOL JNM-ECX400II spectrometer. Powder X-ray diffraction (XRD) analysis was performed by RIGAKU MiniFlex II powder diffractometer using Cu Kα radiation with 35 kV beam voltage and 15 mA beam current. CHN analysis was carried out by PerkinElmer 2400 Series II CHNS Elemental Analyzer. Inductively coupled plasma optical emission spectrometry (ICP-OES) measurements were performed using the PerkinElmer ICP-OES instrument (PerkinElmer, Inc., Shelton, CT, USA). For ICP-OES analysis, Fe_2O_3/HNTs nanocomposite was dissolved in HCl and the supernatant was used to estimate the iron concentration in the composite. Specific surface area was determined by the BET method using nitrogen adsorption/desorption isotherms at 77 K with 3flex Micromeritics analyzer. Zeta potential was measured by Malvern Nano ZS instrument. Magnetization measurement of the sample was done with a vibrating sample magnetometer (VSM), LakeShore 7400 series. UV-visible absorption spectra were obtained at room temperature using a Shimadzu spectrometer, UV-2600 and taking the solutions in a 1 cm quartz cuvette.

Table S1 Assignment of FTIR bands after loading of disodium salt of ethylenediaminetetraacetic acid (EDTA) in halloysite nanoclays.

Wavenumber (cm^{-1})	Assignment	Species
3697	Inner surface -OH group	HNTs
3621	Inner -OH group	HNTs
2945	C–H asymmetric stretching	EDTA
2840	C–H symmetric stretching	EDTA
1655	C=O stretching	EDTA
1585	asymmetric stretching C–O	EDTA
1410	Symmetric stretching C–O	EDTA
1326	C–C stretching	EDTA
1264	C–N stretching	EDTA

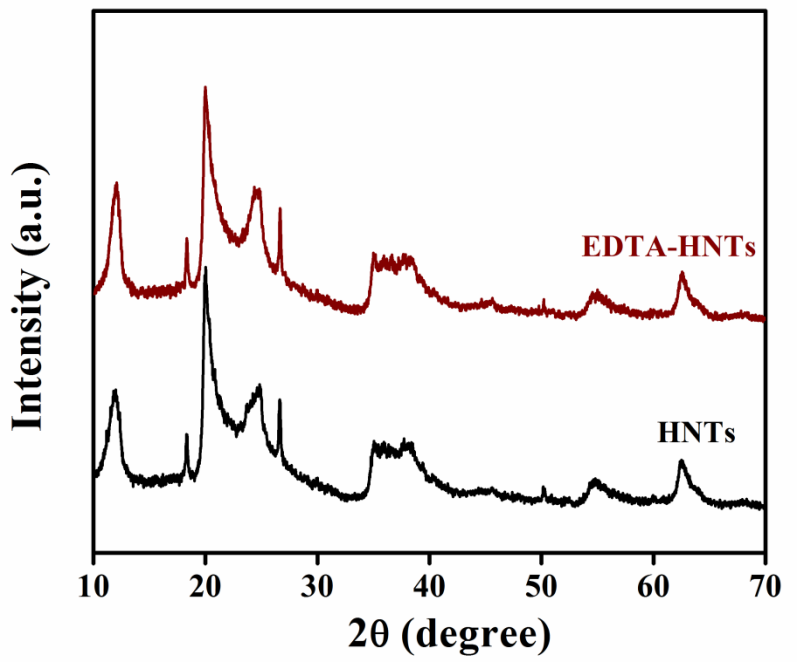

Fig. S1 XRD patterns of bare HNTs and after loaded with ethylenediaminetetraacetic acid (EDTA), indicating the absence of any intercalation of EDTA into the interlayer of tubes wall. The diffraction pattern illustrates the tubular structure of the clay nanotubes because of the observed (020) reflection and the characteristic (001) reflection in EDTA-HNTs remain unchanged, demonstrating the absence of any intercalation of EDTA molecules into the interlayer of tubes wall.

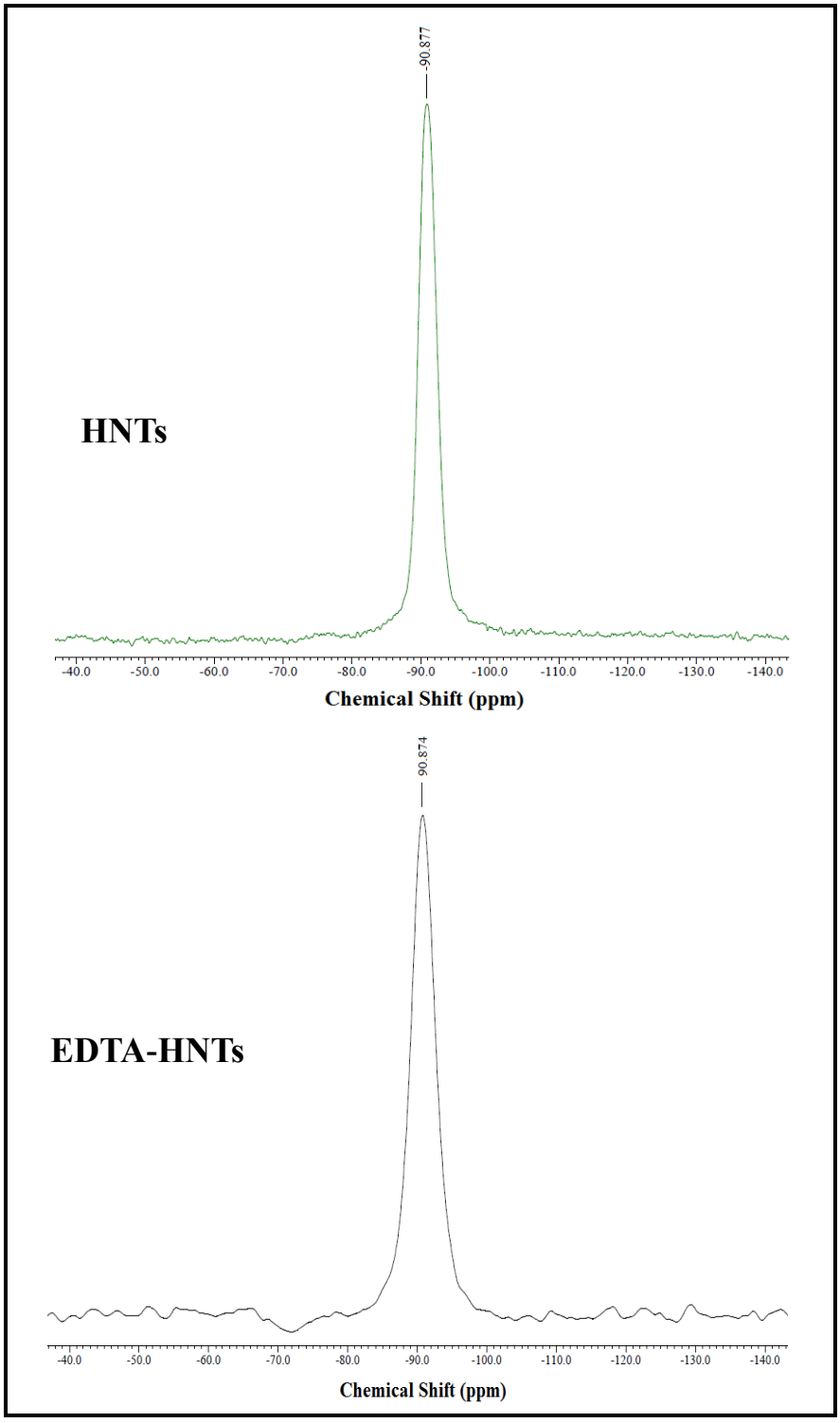

Fig. S2 ^{29}Si CPMAS NMR spectra of pristine HNTs and corresponding EDTA-HNTs respectively. These spectra represent that there is no shift in the resonances at -90.7 ppm originating from silicon and thus eliminate the possibility of binding of EDTA to the outer silica surfaces of HNTs.

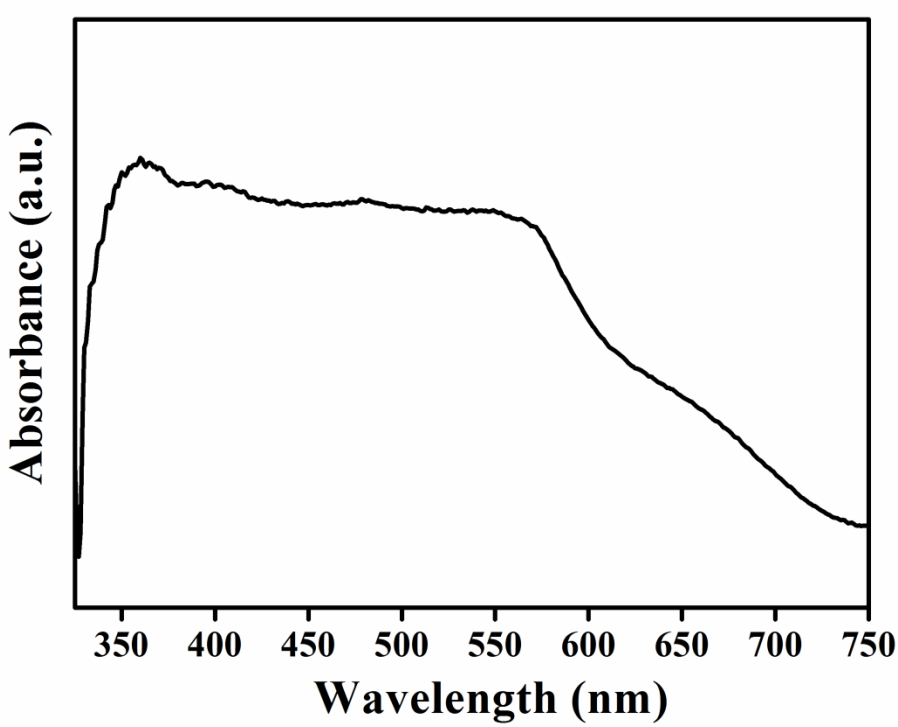

Fig. S3 UV-visible diffuse reflectance spectrum of α-Fe_2O_3/HNTs nanocomposites, demonstrating two peaks at 360 and 556 nm correspond to $^6A_1 \longrightarrow {}^4E$ and $2(^6A_1) \longrightarrow 2(^4T_1)$ ligand field transition of Fe (III) respectively.

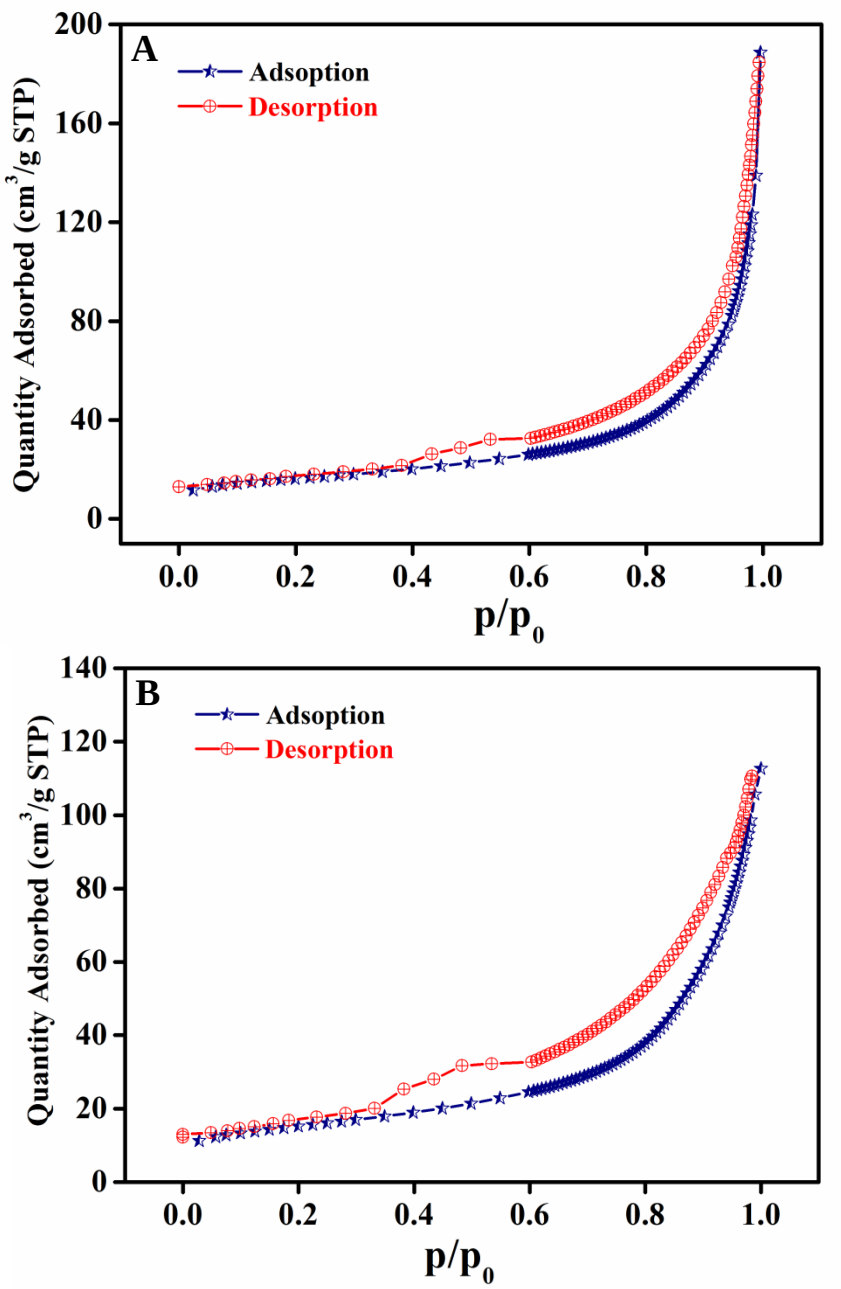

Fig. S4 Nitrogen adsorption/desorption isotherms of (A) pristine halloysite and (B) α-Fe_2O_3/HNTs NCs at 77 K.

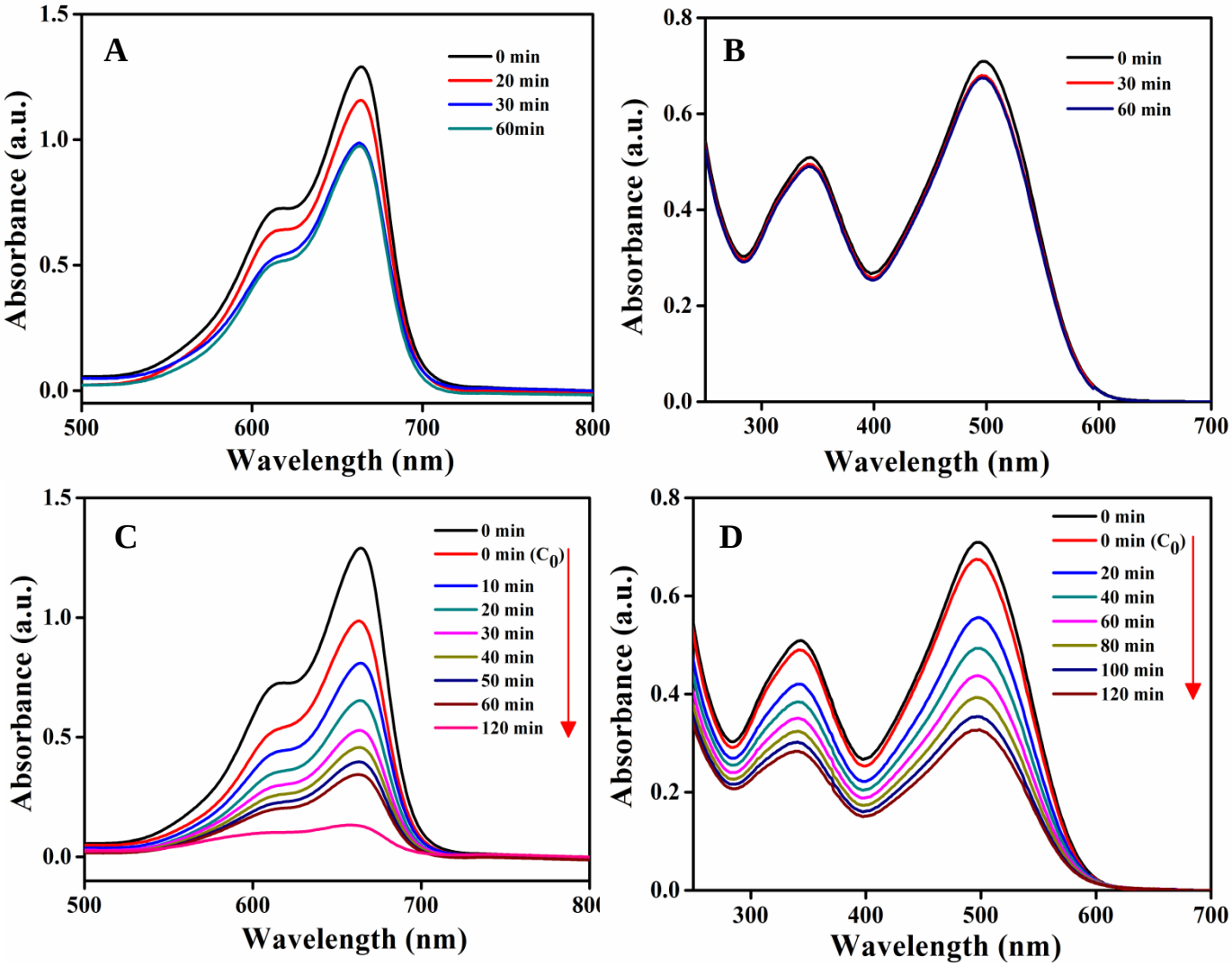

Fig. S5 UV-Visible absorption spectra for the adsorption−desorption equilibrium study of (A) MB and (B) CR as a function of time. After the equilibration, the concentration of the dye solution was considered as the initial concentration (C_0) of the dyes. UV-Visible absorption spectra for the successive degradation of (C) MB and (D) CR under irradiation of sunlight in presence of α-Fe_2O_3/HNTs NCs.

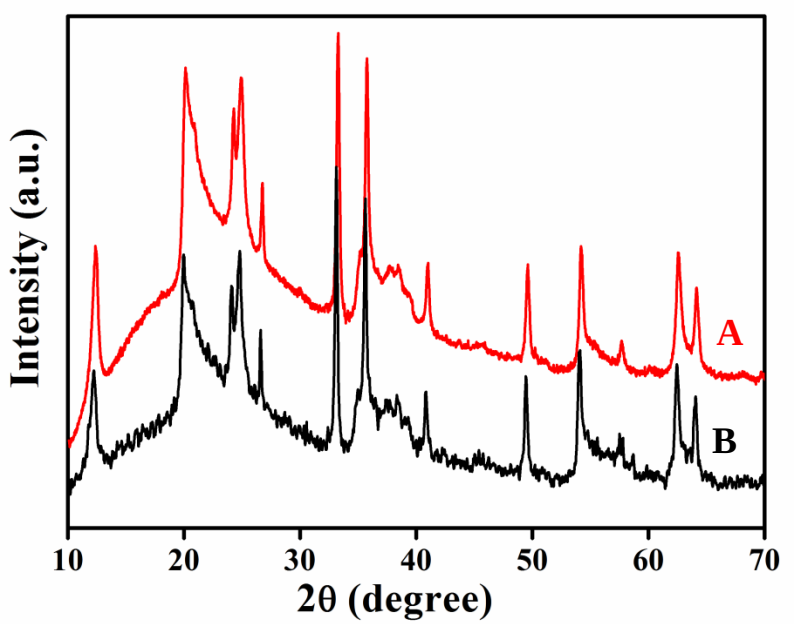

Fig. S6 XRD patterns of α-Fe_2O_3/HNTs nanocomposites (A) before and (B) after the end of the photodegradation reaction, demonstrating no change in their diffraction pattern.

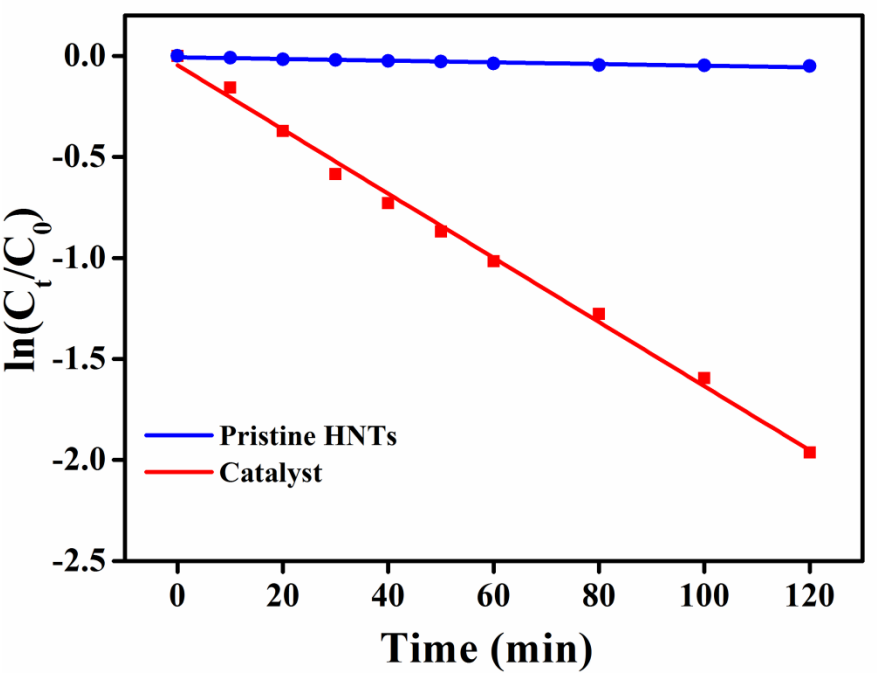

Fig. S7 Degradation of MB under the illumination of sunlight using pristine HNTs and α-Fe_2O_3/HNTs nanocomposites respectively.

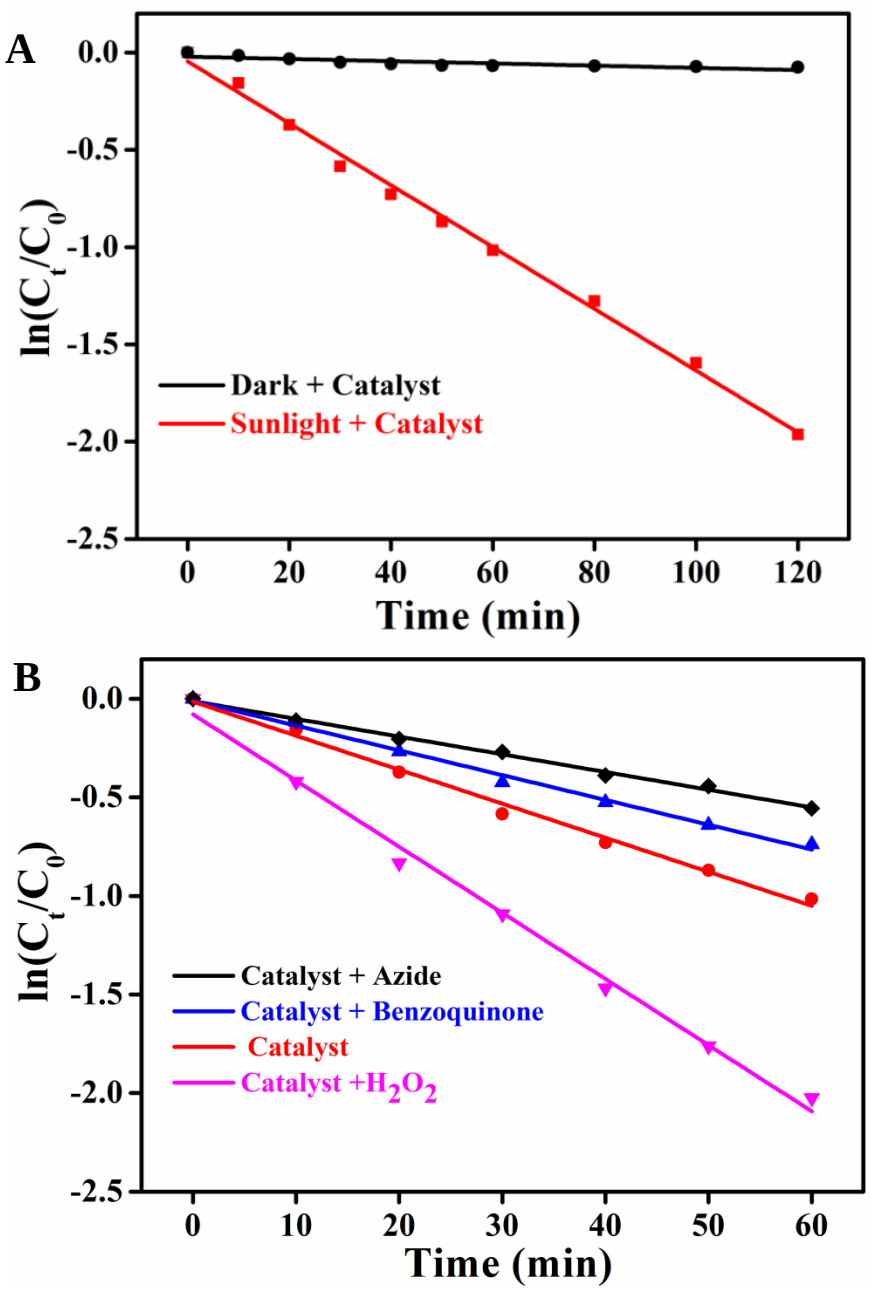

Fig. S8 Comparison of degradation rates of MB (A) in dark and under sunlight illumination in presence of catalyst. (B) Comparison of degradation rates of MB under sunlight illumination in presence of catalyst and/or H_2O_2, sodium azide and 1,4-benzoquinone respectively to demonstrate that the degradation of MB proceeds through the photocatalytic pathway via the formation of reactive oxygen species.